QUANTIFYING SURFACE FLUXES IN THE ICE-COVERED POLAR OCEANS USING SATELLITE MICROWAVE REMOTE SENSING DATA

Mark R. Drinkwater* and Ronald Kwok
Jet Propulsion Laboratory
California Institute of Technology

Jim A. Maslanik, Chuck W. Fowler and W.J. Emery
University of Colorado

Cathleen A. Geiger
Center for Climatic Research
University of Delaware

ABSTRACT - *Satellite passive microwave sea ice concentration data of 20 or more years in extent have become an important proxy for climate variability. More recently, in the 1990's these data have been exploited in conjunction with fine resolution satellite image datasets originating from ERS-1/2, and RADARSAT Synthetic Aperture Radar (SAR), and new medium resolution ERS-1/2 and NSCAT radar scatterometer instrument data. New technologies in image data processing and sea-ice tracking developed from these efforts are generating fresh insight into the dynamics and evolution of the Arctic and Southern Ocean ice covers. These approaches have matured to the point where estimates of salt and freshwater exports can be made, as well as assessments of the impact that these have upon the thermohaline circulation.*

1. INTRODUCTION

A detailed knowledge of sea-ice drift dynamics is necessary for understanding climate processes operating at the air-ice-ocean interface in the polar oceans. Although thermodynamics controls the ice growth process, dynamics affects the displacement and dislocation of the ice cover, thereby limiting the geographic distribution of exposed open water in lead fractures and polynyas. In this manner, opening and closing of the sea-ice pack in response to differential motion essentially regulates the spatial and temporal variability in ocean-atmosphere exchange processes. Furthermore, it modifies momentum transfer to the upper ocean, the local exchange of turbulent sensible and latent heat, the input of solar energy, ice formation and brine production, and the ice-thickness distribution.

A seasonally evolving sea-ice cover also has a significant impact on water-mass modification processes, particularly in the Greenland Sea in the Northern Hemisphere and in the Weddell and Ross Sea basins in the Southern Hemisphere. In these key regions, ice formation and seasonal melting influence upper-ocean stability by changing he horizontal and vertical salinity and buoyancy gradients. Vigorous localized ice formation can induce convective overturning, or alternately seasonal melting can stabilize the mixed layer. Both can have an impact on key processes driving the global thermohaline ocean circulation. On longer time-scales, large-scale sea-ice advection controls the redistribution of freshwater. Sea ice advected to lower latitudes provides an important contribution to the rate of freshening of the surface waters, particularly in locations which can determine the intensity of the thermohaline circulation (Aagaard and Carmack, 1989).

Traditionally, instrumented buoys [Thorndike and Colony, 1980a; Kottmeier and Sellman, 1996] and models [Baranov *et al.*, 1976, Harder *et al.*, 1998] have been deployed to try to understand large-scale sea-ice dynamic processes. Arctic buoy deployments continue through the International Arctic Buoy Program [Thorndike and Colony, 1980b]. But, until recently Antarctic drifting buoy deployments were not coordinated and are more limited in time and space [Drinkwater *et al.*, 1999]. Using the latter data, it remains difficult to accurately quantify seasonally varying basin-scale ice dynamics and surface forcing experienced by the Southern Ocean ice cover, or to validate the new generation of fine-resolution coupled ice-ocean models.

* Principal Author's Address: Jet Propulsion Laboratory, California Institute of Technology,
Mail Stop 300-323 4800 Oak Grove Drive, , Pasadena, CA 91109-8099, USA.
Tel: 818-354-8189; Email: m.drinkwater@jpl.nasa.gov; URL: http://polar.jpl.nasa.gov

Recent satellite remote sensing studies of Arctic and Antarctic sea-ice dynamics have started to highlight the extremely dynamic nature of the polar sea-ice cover, together with characterizing its varied spatial and temporal response to climate forcing. A number of innovative technologies are being applied to all weather day and night active and passive microwave remote sensing datasets in order to track sea-ice floe trajectories on a variety of time and space scales [Fily and Rothrock, 1987, Kwok *et al.*, 1990; Emery *et al.*, 1991; Liu and Cavalieri, 1998]. Individual ice floes and regional assemblages of ice floes may be followed using these pattern recognition approaches to yield gridded Eulerian or Lagrangian ice kinematics datasets. SMMR and SSM/I satellite radiometer instruments together yield a record extending 20 years from 1978 until 1998, while overlapping combined radar and radiometer datasets exist from 1991 until the present day.

Radar and passive microwave radiometer data are used here in conjunction with meteorological analysis fields and in-situ drifter data to investigate the seasonal to interannual variability in bipolar sea-ice dynamics over the period 1978 - 1998. Supporting field data from the 1992 Ice Station Weddell drift in Antarctica and 1997/8 SHEBA Arctic experiment are used as validation of the satellite results. A variety of surface measurements were made during these experiments, along with deployment of drifting buoys. Together these contribute to the validation of satellite surface measurements, and the construction of optimally interpolated fields of ice drift tracking results.

2. SEA-ICE RESPONSE TO CLIMATE VARIABILITY

The long term ice concentration record from passive microwave satellites have been the traditional 'staple diet' of polar ice research over the last two decades. The extensive climate record now available from these combined satellite measurements has enabled development of monthly anomaly records of total ice area and ice extent for both hemispheres [Cavalieri *et al.*, 1997]. Results in Figure 1 confirm reductions of area and extent in the Northern Hemisphere previously described by Maslanik *et al.*, (1996) and Johannessen *et al.* (1995). In contrast, a slight increase is observed in the Southern Hemisphere, implying

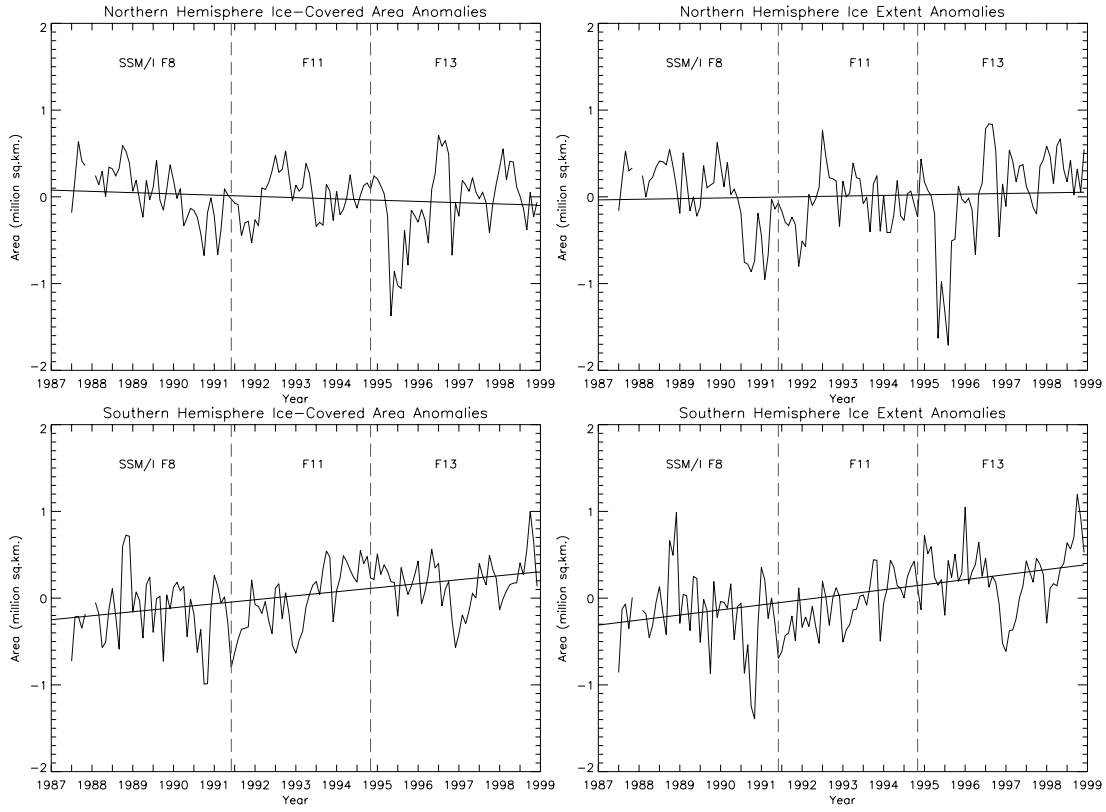

Figure 1. Monthly sea ice area and extent anomalies for the Arctic and Antarctic regions, extracted using the Standard NASA Team Algorithm (Gloersen *et al.*, 1992).

an asymmetry in hemispheric ice cover previously simulated in response to increasing atmospheric CO_2 [Manabe *et al.*, 1992]. Large negative summer anomalies in both area and extent imply significant warming and melting events that remove large portions of the hemispheric ice cover. These are apparent in the summers of 1990 and 1995 in the north and the late autumn of 1990 and summer of 1996/97 in the south. Despite such large negative anomalies in each of these years, the sea ice system has a remarkable capability to restore balance in only one or two years following each event. In this paper, we use contemporary datasets to illustrate the value and applicability of large-scale sea-ice motion and dynamics in studies of the polar sea-ice response to seasonal and interannual forcing. Since both ice area and extent respond in a well correlated fashion, this implies that sea ice drift dynamics play a fundamental role not only in controlling ice concentration and distribution, but also in regulating the ocean-atmosphere fluxes providing the restoring capability.

3. SEA-ICE DRIFT TRACKING

Pattern recognition techniques have matured over the last several years for processing pairs of satellite radiometer and radar images into gridded ice motion data. Datasets to which these techniques have successfully been applied include SSM/I passive microwave data [Agnew *et al.*, 1998; Emery *et al.*, 1997; Kwok *et al.*, 1997; Maslanik *et al.*, 1998; and Liu and Cavalieri, 1998], ERS-1/2 and NSCAT scatterometer data [Drinkwater, 1997; Long and Drinkwater, 1999; Liu *et al.*, 1999], and Synthetic Aperture Radar (SAR) data from ERS-1/2 [Stern, *et al.*, 1995; Drinkwater, 1998a,b; Li *et al.*, 1998] and RADARSAT [Kwok *et al.*, In Press].

Sea ice drifts largely under forces imparted by the wind, ocean currents, and internal ice stresses on time scales longer than 1 day. During seasons of the year when ice concentrations are low, the internal forces in the ice cover may be negligible and the principal balance of forces is between wind and water stresses, sea surface tilt and the Coriolis force [Thorndike and Colony, 1982]. Until recently, ARGOS buoy location precision made it difficult to resolve sub-daily ice motion fluctuations (and thus short-term differential motion) to a great degree of accuracy [Geiger *et al.*, 1998]. Results of analysis of more recent GPS buoy data from Ice Station Weddell indicate that many temporal scales are involved in the 'forced' response of the sea-ice cover, particularly on continental shelf regions, where tidal ice dynamics regulate air-sea fluxes, high-salinity shelf-water production and processes influencing the thermohaline circulation.

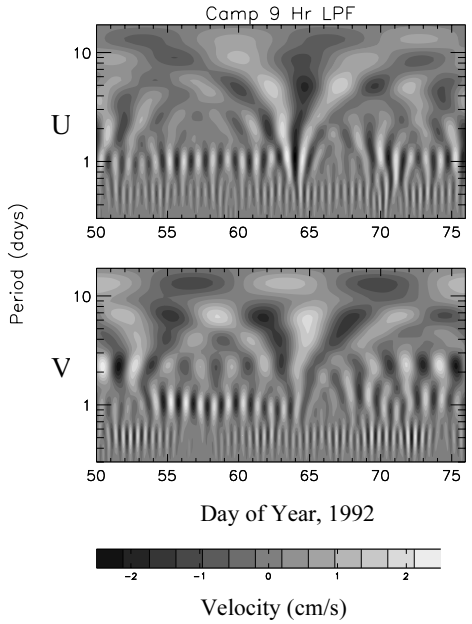

Figure 2. Periodograms of low-pass filtered u and v ice velocity components for Ice Station Weddell, for the period day 50 to day 76. The vertical axis indicates the period of the fluctuations and the intensity shows the velocity on a scale -2 (black) to 2 cm/s (white).

Figure 2 indicates that complex non-linear interactions exist between a variety of frequencies of ice drift. A range of periods of ice motion are recovered from the data record, comprising semi-diurnal and diurnal tides (at 2 and 1 cycles/day, respectively), up to synoptic storm forcing at several day periods and longer (> 0.1 cycles/day). The dominant frequencies and highest energy variability in this time series is observed in the semi-diurnal and diurnal tidal bands [Geiger *et al.*, 1998]. At the top of each periodogram, the lowest frequency variability is resolved at periods exceeding 15 days, with some of the low frequency activity linked with spring/neap tidal activity at a period of 327.9 hours (~ 2 weeks). What is interesting about Figure 2 is the way all frequencies resonate on or around day 64 during a large storm system over the ice station. Although the u/v components of velocity are observed to oscillate, all periods move into and out of phase as the storm approaches and then retreats. This is observed as the continuous light and dark bands converging downwards upon day 64.

Ice Station Weddell buoy array measurements made in conjunction with Figure 2 show that the highest energy strain activity occurs precisely when tidal currents, wind stress and ocean current stresses all act in concert [Geiger *et al.*, 1998]. During these events the largest deformation takes place in the ice cover. Unfortunately, large-scale SSM/I satellite ice motion products can only presently provide us with lower frequency/long period synoptic response of the ice cover to the meteorological forcing patterns due to orbital constraints upon sampling. When combined with in-situ buoy data, only high temporal revisit frequency SAR data can be used to quantify tidal or inertial influences on sea-ice dynamics and new ice growth on the continental shelves. This is the topic of ongoing research by Drinkwater and Geiger (NSF Approved Study OPP 9818645).

Since buoys are necessary to resolve some frequency components of this short-term variability, this result highlights significant deficiencies in the historical buoy records of sea-ice drift. Large areas with significant tidal and inertial signals are poorly sampled in time and space. These regions presently include the Kara Sea, Hudson Bay, Baffin Bay, Bering Sea, Sea of Okhotsk, and the majority of the Southern Ocean. Future buoy deployments by the International Arctic Buoy Program (http://iabp.apl.washington.edu/) and the recently established International Antarctic Buoy Program (http://www.antcrc.utas.edu.au/antcrc/buoys/buoys.html) should, together with satellite-derived ice motion products, strive to fill these gaps in our understanding [Drinkwater *et al.*, 1999].

4. LARGE-SCALE ICE DRIFT

The accuracy and performance of large-scale Arctic and Antarctic ice motion retrievals from SSM/I and NSCAT images have been considered through quantitative comparisons with drifting buoys [Kwok *et al.*, 1998; Liu et al, 1999; Drinkwater and Liu, 1999; and Geiger *et al.*, In Press], to a lesser degree with other satellite drift products derived from SAR and NSCAT [Drinkwater, 1997; Liu et al, 1999], and with model simulations. Comparisons with ECMWF and NCEP pressure field data in both hemispheres [Kwok *et al.*, 1998; and Drinkwater and Liu, 1999] confirm that sea-ice drift is forced predominantly by pressure-gradient winds in response to the large-scale sea-level pressure (SLP) pattern (Figure 3). Synoptic scale sea-ice drift adjusts rapidly to changes in wind forcing on time scales of 12 hours or less depending on the location with respect to the coastline [Drinkwater, 1998a].

The primary limitation of SSM/I large-scale drift data is that they can only capture synoptic variability on time scales of days. Results shown in Figure 3 indicate 3-day ice motion from 8-11 March, 1993 in

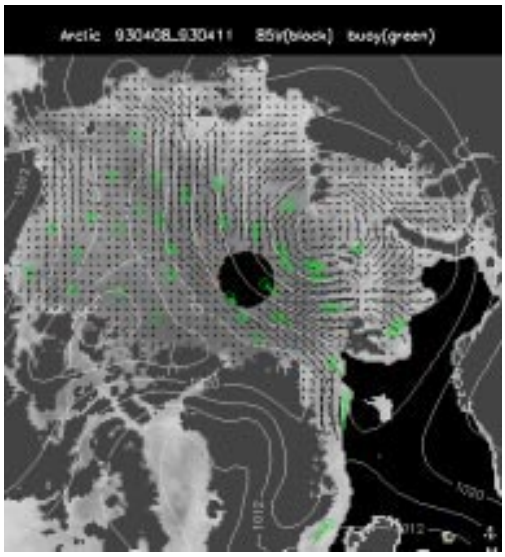

Figure 3a. SSM/I 85 GHz-derived Arctic ice drift from 8-11 April, with IABP buoy drift vectors superimposed.

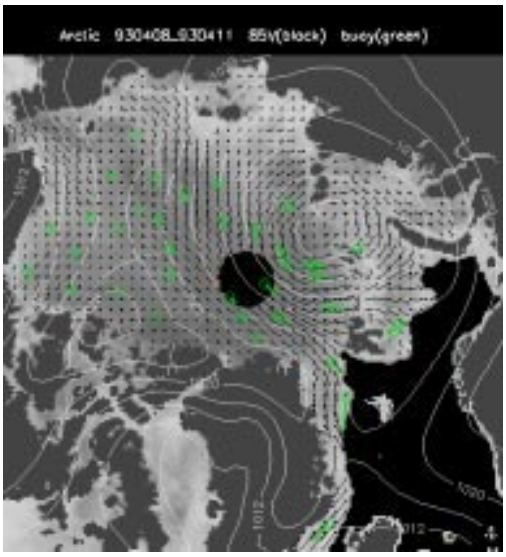

Figure 3b. Same as 3a but with optimal interpolated ice motion incorporating buoy data.

response to a large low pressure system centered near Severnaya Zemlya in the Kara Sea. IABP buoy vectors are highlighted in green to indicate the correspondence with the SSM/I 85 GHz-derived drift. Drift vectors highlight the way in which the ice follows the isobars. This highly variable pattern of large-scale sea-ice dynamics has a significant impact upon ice transport from the East Siberian and Laptev Seas across the Arctic Basin. The Transpolar Drift Stream, as it is known, results in export of salt and freshwater out of the Arctic Ocean through the Fram Strait into the Greenland Sea [Emery *et al.*, 1997]. The contribution of ice advection to these export terms is considered in a later section.

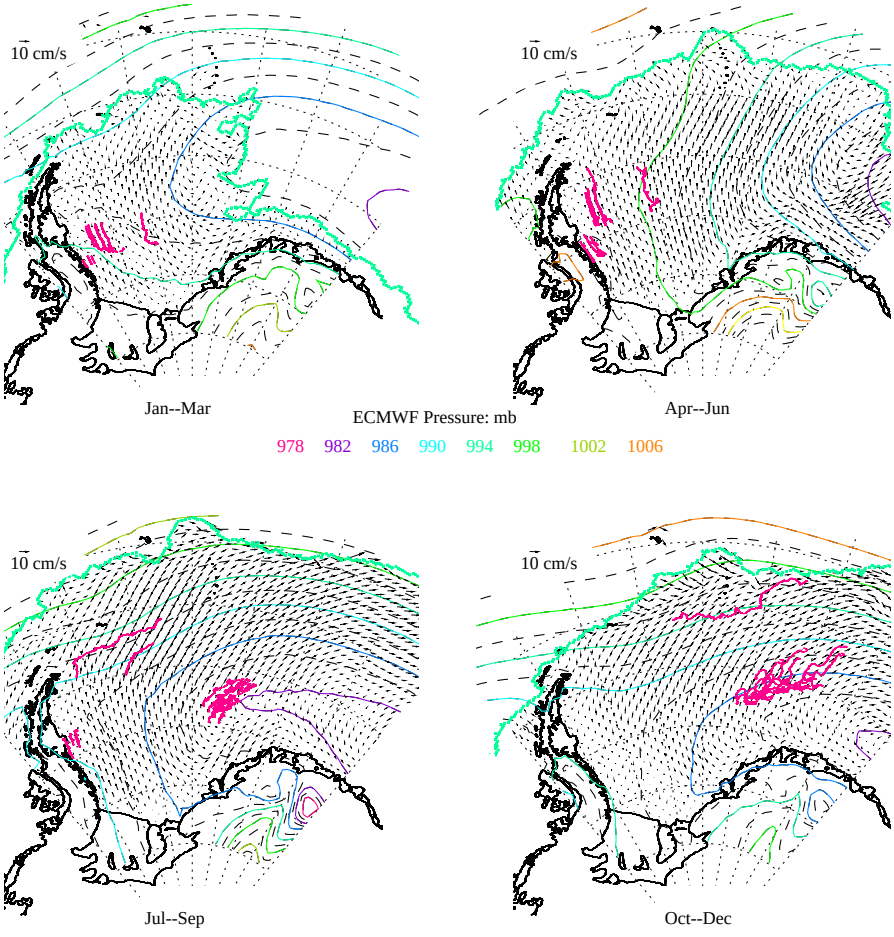

Figure 4. Seasonal variability Weddell Sea 1 day ice drift in 1992, together with simultaneous buoy drift trajectories [courtesy IABP participants] and mean ECMWF SLP contours in hPa. Ice motion was derived from SSM/I 85 GHz data.

The primary limitation of SSM/I large-scale drift data is that they can only capture synoptic variability on time scales of days. Results shown in Figure 3 indicate 3-day ice motion from 8-11 March, 1993 in response to a large low pressure system centered near Severnaya Zemlya in the Kara Sea. IABP buoy vectors are highlighted in green to indicate the correspondence with the SSM/I 85 GHz-derived drift. Drift vectors highlight the way in which the ice follows the isobars. This highly variable pattern of large-scale sea-ice dynamics has a significant impact upon ice transport from the East Siberian and Laptev Seas across the Arctic Basin. The Transpolar Drift Stream, as it is known, results in export of salt and freshwater out of the Arctic Ocean through the Fram Strait into the Greenland Sea [Emery *et al.*, 1997]. The contribution of ice advection to these export terms is considered in a later section.

Seasonal to interannual comparisons between Antarctic gridded SSM/I ice-drift vectors and ECMWF or NCEP analyses (Figures 4 and 5) indicate that daily, or longer time-scale large-scale sea-ice circulation

around Antarctica, is governed by the seasonally varying mean, synoptic pressure pattern. Figure 4 shows the seasonal evolution in the ice drift pattern in the Weddell-Enderby basin in response to typical synoptic low pressure centered east of the Greenwich meridian. As the ice margin (highlighted in green) advances, the basin fills with ice and the pattern of the Weddell Gyre emerge. At the same time, internal stresses are translated through the ice cover from the coasts, resulting in larger shear stresses along the coastal belts. Other key characteristics of Figure 4 are the cyclonic (clockwise) gyre motion and the acceleration of the sea ice as it escapes the coastal entrapment of the Antarctic peninsula to drift rapidly eastwards in the Antarctic Circumpolar Current (ACC). Also evident is a source of ice entering the Weddell Sea, carried by the coastal East Wind Drift.

Figure 5 captures the three primary Antarctic gyre circulations driven by the typical wavenumber 3 pattern in SLP. Significant interannual variability is evident in Antarctic-wide ice drift, with large contrasting extremes in ice motion evident in 1988 and 1990 in response to changes in the synoptic pressure patterns. In 1988, for instance, exaggerated meridional ice transport appears connected to the development of a wavenumber 2 pattern in SLP, with a strengthening of the Ross Sea and coalescence of the two East Antarctic lows into a single low pressure center at 70^{o}E. Strong zonal gradients of SLP in

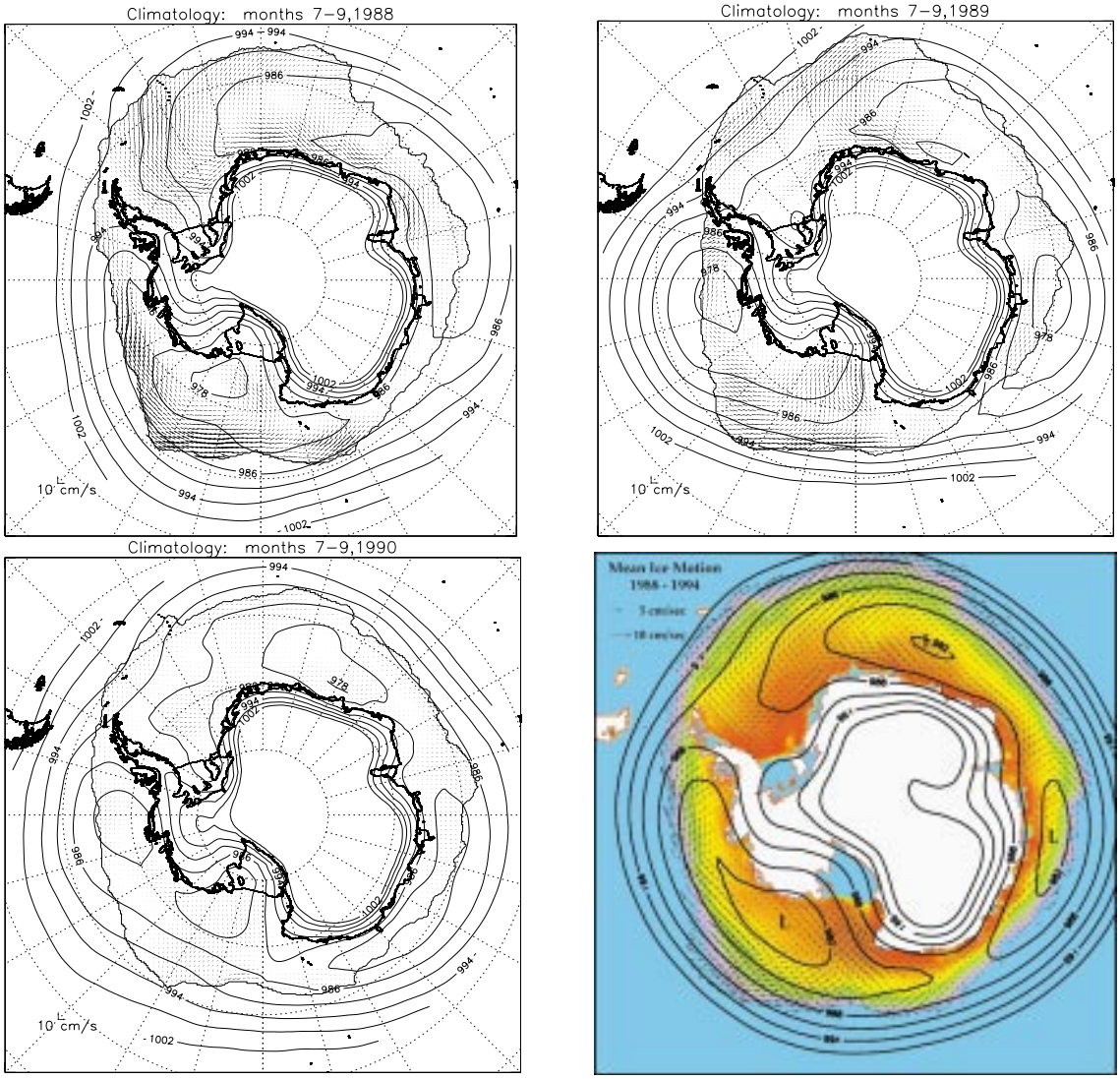

Figure 5. Interannual variability in winter (Jul. - Sept.) mean daily Antarctic ice drift from SSM/I 85.5GHz data for (a) 1988; (b) 1989; and (c) 1990, with mean SLP contours. Panel (d) shows the 1988-1994 mean. Colours in panel (d) indicate ice concentration.

the Weddell and Ross Seas contribute to the large positive seasonal ice extent anomaly apparent in Figure 1 in the latter part of 1988. In contrast, more sluggish meridional ice transport in 1990 appears linked to the strong end of year negative anomaly in Figure 1, and the early summer ice edge retreat in summer 1990/91 noted by Jacobs and Comiso (1997). During this summer, the strength of the anomalous low-pressure center (already evident in Figure 5) resulted in enhanced warm air advection, in the manner described by Garreaud and Battisti (1999).

Discrepancies have been found in some comparisons of ECMWF and NCEP SLP analysis products with the buoy drift data, which indicates errors in the computation of the surface pressure fields by the analysis models. This is most apparent in the Southern hemisphere seasonal climatologies in Figure 4 and the winter mean SLP and drift fields in Figure 5. Discrepancies are manifested as a displacement of the 'apparent' centers of cyclonic gyre circulations away from the closed contours of the SLP fields (such as the low pressure center over the Ross Sea in 1994), or as details of the mean motion fields not apparent in the pressure fields.

5. OPTIMALLY INTERPOLATED ICE DRIFT FIELDS

Many of the shortcomings of existing coupled ocean-ice-atmosphere models, with respect to simulation of the polar oceans ice cover, can be identified and addressed with a gridded ice dynamics data set. Since polar buoy deployment resources are finite and relatively limited, the ideal approach to generating these data incorporates a blend of buoy and satellite data to expand the spatial and temporal coverage and to assess the effects of motion at different scales [Geiger *et al.*, 1998; Drinkwater *et al.*, 1999]. The proposed objective is to continue to coordinate future drifter deployments whilst also generating an historical archive of buoy deployments over the period of contemporary passive microwave satellite data. In-situ observations alone, however, provide only a limited spatial and temporal sample of surface transports. For this reason, optimal interpolation of both satellite- and buoy-derived ice drift datasets has been proposed [Drinkwater *et al.*, 1999] so that the resulting fields may be assimilated as boundary conditions in climate simulation models.

Liu *et al.* (1999) have made initial efforts to merge different satellite motion products with buoy data. Figure 6 shows satellite-derived daily drift fields on complementary time scales from SSM/I, and the NASA scatterometer (NSCAT) on board ADEOS-I. Both offer spatial resolutions exceeding 20 km, and daily bi-polar sea-ice coverage. The advantage of the Ku-band (13.6 GHz) radar-derived motion fields is that it does not experience the problems caused by water vapour in the SSM/I 85.5 GHz channel. In this manner, NSCAT is exploited to fill in the poorly tracked regions, particularly in locations and seasons where the weather influence prevents successful or accurate SSM/I tracking.

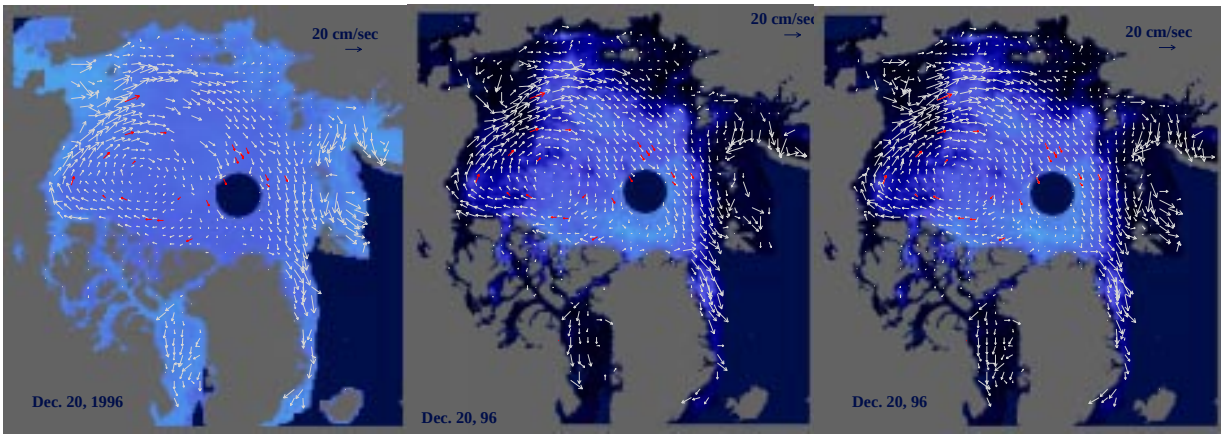

Figure 6. Daily sea-ice motion vector field for December 20, 1996 from (a) 85.5 GHz SSM/I; (b) 13.6 GHz NSCAT; and (c) merged SSM/I and NSCAT data set. Buoy motion vectors are shown in red [after Long and Drinkwater, 1999].

Lower frequency radar data are therefore necessary to reduce seasonally dependent weather problems evident in ice motion tracking using 85.5 GHz SSM/I image data. The ideal candidate for this purpose is presently the SeaWinds (13.6 GHz) scatterometer on board QuikScat, which generates daily full polar images at approximately 4 km resolution. [Long and Drinkwater, 1999] We propose that daily SeaWinds ice motion products be generated and merged with SSM/I motion and buoy data following similar methods to that described by Liu *et al.* (1999). The gridded ice drift measurements can then be objectively analysed (with different weightings applied to each data set) to generate an interpolated product similar to Figure 3b. The advantage of this procedure is a gap-filled gridded motion field for assimilation into models.

6. LAGRANGIAN TRACKING

Recent developments of Lagrangian ice tracking permit precise quantification of the differential kinematics and thus opening and closing of the sea ice pack over the entire Arctic basin [Kwok *et al.*, 1995]. The RADARSAT Geophysical Processor System (RGPS), installed at the Alaska SAR Facility, computes ice motion on a Lagrangian grid from composite SAR image swath maps acquired as a "weekly snapshot" of basinwide ice conditions. A Lagrangian tracking and gridding procedure allows ice properties within each grid cell to evolve as they are tracked in time. Together with a simple ice-growth model (driven by air temperature), the ice is allowed to thicken and age as it drifts [Kwok *et al.*, 1995]. Divergence and shear events that cause opening of leads are treated by allowing new ice to grow in the open-water fraction of those grid cells. Simple thermodynamics control the growth rate and incremental thickness increase between each weekly time step. Conversely, convergence within a grid cell is treated as ridging of the thinnest component of the thickness and age distribution. The overall distribution of ice thickness is then adjusted by redistributing that area of ridged thin ice into the ridged category. Figure 7 shows a result of tracking the 16-22 December ice motion in 1996. The individual x and y components of motion are computed (referenced to the SSM/I polar stereographic projection) together with the differential kinematic parameters: divergence, shear and vorticity.

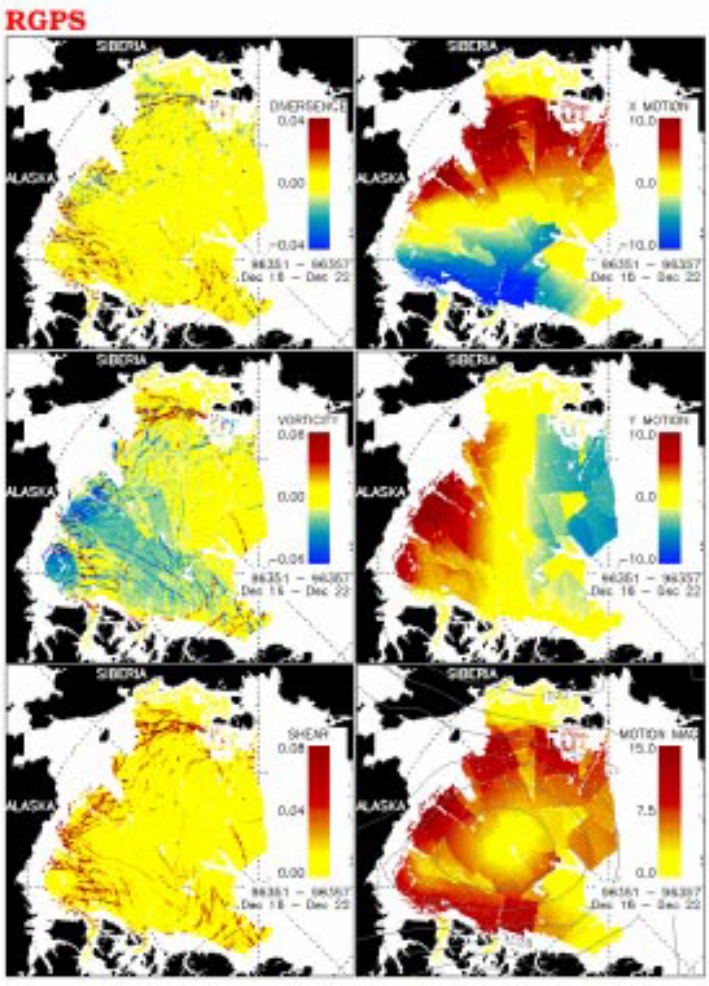

Figure 7. Divergence, vorticity, shear and general ice motion from Dec 16, 96 - Dec 22, 96 (96351 - 96357), extracted from the RADARSAT Geophysical Processor, at the Alaska SAR Facility.

Lagrangian calculations allow the sea-ice growth in leads and the resulting salt flux to be more accurately quantified. Gridded ice deformation measurements also facilitate estimates of the evolving ice-thickness distribution and the proportion of ridging within each grid cell. Figure 8 illustrates the thin and ridged ice-thickness distribution that are calculated by the RGPS for 22 December 1996. The spatial distribution of thin ice, and its correspondence with small-scale shear, vorticity and divergence (in Figure 7) underlines the importance of making both precise and

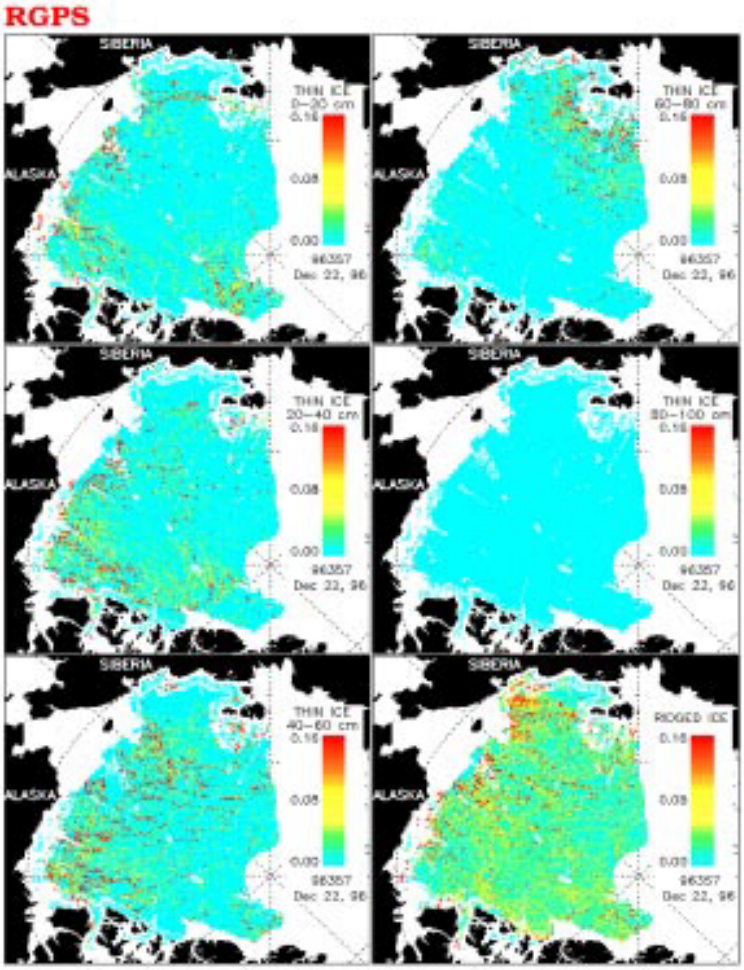

Figure 8. Ice thickness distributions on December 22, 1996 (96357) represented as the binned fraction of thin ice in each grid cell.

accurate measurements of Arctic basin-wide ice deformation using high-resolution SAR.

The link between fracturing and ridging is evident in Figures 7 and 8. New ice growing in lead openings provides the weakest material for building ridged ice under subsequent ice convergence and compression. The areal proportion and spatial distribution of thin ice growing in leads also exerts an important control upon ocean-atmosphere heat fluxes. Products from the RGPS will be essential to developing more accurate calculations of the area-weighted ocean-ice-air heat fluxes.

7. COMBINING SATELLITE AND IN-SITU DATA IN FLUX ESTIMATES

Satellite-derived, gridded ice-motion examples in the previous sections demonstrate the large-scale response of sea-ice drift in the Arctic basin and Southern Ocean to atmospheric forcing on a variety time and space scales. For the first time, this presents the opportunity to directly assess the mass balance of the sea-ice cover and to quantify the freshwater and salt redistribution terms which sea-ice advection represents. The net horizontal and vertical advective components of freshwater flux at the ocean surface may be accurately quantified by measuring the following terms of the salt/freshwater balance

- Advective ice transport across an instrumented flux gate
- Local melt rate
- Local ice growth

The first of the three terms may be estimated by combining satellite-derived Eulerian ice motion across the flux gate L_{gate} with Upward Looking Sonar ice draft measurements H_{ice}. The product of the two time-series may be used to obtain the ice volume flux Ψ_{ice}, where

$$\Psi_{ice}(t) = \int_0^{Lgate} V_{ice}(t) \times H_{ice}(t) \; dx \,. \tag{1}$$

This quantity may be translated into the mass transport with a small error, by multiplying Ψ_{ice} by a typical mean ice density of ρ_{ice}= 910 kg m^{-3}. The corresponding salt transport term M_{salt} is then simply

$$M_{salt}(t) = \Psi_{ice}(t) \times \rho_{ice} \times S_{ice}\,, \tag{2}$$

where S_{ice} is the mean salinity of the sea ice. Seasonally-varying *in-situ* melt is typically comprised of basal melting due to ocean heat flux, and lateral melting due to short-wave radiative input to leads. The ocean heat flux is typically quantified using moored CTDs that are ideally attached to the same mooring

as the ULS instrumentation. The two last terms comprising melt and local ice growth are then typically estimated using simple thermodynamic models.

7.1 Arctic Ice Export

Arctic-wide results contribute to new insights into the sea-ice mass balance of the Arctic basin and the resultant interannual variability in the freshwater flux into the North Atlantic in response to northern hemisphere atmospheric variability. Kwok and Rothrock (1989) studied the variability of Arctic ice export and the North Atlantic Oscillation (NAO) index (i.e. Lisbon - Iceland normalised pressure difference) and found a significant correlation between ice area flux and the intensity of the Icelandic low. Annual means of satellite ice drift velocity measurements for the December through March period led to the Fram Strait area flux time series shown in Figure 9. The Fram Strait flux gate concept allows the area advection term into the North Atlantic to be computed to known accuracy. 'In situ' melt rates and ice draft time-series are then derived from a series of Norwegian moorings with CTD chains and ULS sensors [Vinje and Finnekasa, 1986; Vinje *et al.*, In Press]. Upward ocean heat flux is precisely quantified and the time-varying ice thickness derived at the flux gate location.

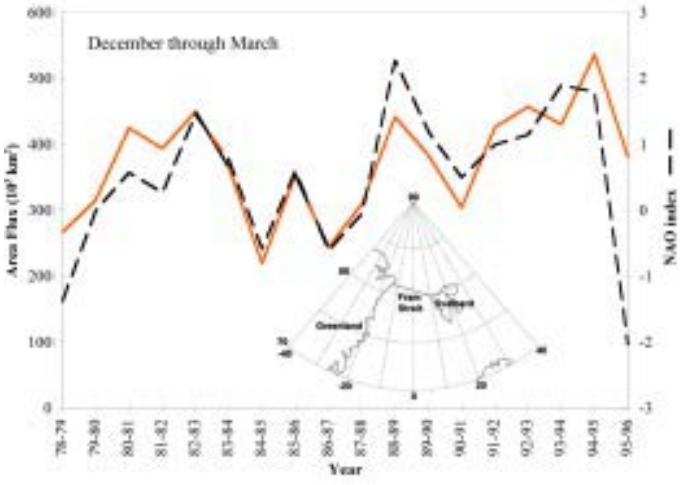

Figure 9. Comparison of Fram Strait December - March integrated ice area fluxes and North Atlantic Oscillation (NAO) index [after Kwok and Rothrock, 1999].

The mean melt-water contribution to the Greenland Sea is computed by Rudberg *et al.* (1999) for the period July 1992 through Jun 1997 (their Figure 1). The volume flux of ice through the Fram Strait gate (Figure 9) decreases almost linearly with latitude as one moves south from the flux gate at 80° N. Winter fluxes (Oct-Mar) decrease from a maximum of 240 km^3/month, to a minimum of 115 km^3/month at 75° N. Stronger winter atmospheric circulation results in more rapid winter ice export, and downstream fluxes which are twice as large as the summer period (Apr- Sept). The downstream distribution of melt water input to the upper ocean depends on the seasonal melt rate at a each latitude as well as the advected supply of thick ice. Melting during the winter months (Nov-Mar) is more vigorous than that during the spring (Apr-Jul), due to stirring of the upper ocean under the more rapid winter ice drift conditions. The thermal barrier effect of strongly stratified conditions during the summer melt period effectively reduces summer freshwater input by a factor of 2 despite summer melt rates that are double those experienced in winter. In general, the ocean heat flux increases towards south, resulting in a latitudinally and seasonally fluctuating melt input to the upper ocean. A minimum net freshwater input of approximately 15 km^3/month is observed close to the flux gate, and the seasonal variability is of the order of 5 km^3/month about this winter mean value. Moving south to a latitude range of 77-76° N the net mean freshwater input increases by a factor of 5 to a value of around 50 km^3/month, with a seasonal variability from 30 to 70 km^3/month.

These results clearly show that SLP variability driven by NAO can either exaggerate or reduce the export of ice from the Arctic basin. The computations are reasonably consistent with simulated ice transport values across 80° N, which showed a 7-year mean value of 0.086 +/- 0.018 Sv, or 225 km^3/month (approx. 2700 km^3/yr) between 1986 and 1992 [Harder *et al.*, 1998]. Here, the combination of satellite and in-situ datasets demonstrate that the combined year to year variations in the ice transport through Fram Strait are of the order of 130% (1000 km^3) of the long-term mean transport, or about half the estimated value of the Great Salinity Anomaly [Dickson *et al.*, 1988; Hakkinen, 1999]. The implications of the above results are significant, given the importance of the North Atlantic region for convective overturning, and ventilation and cooling of the deep waters.

7.2 Weddell Sea Ice Export

Results from Harms (In Press) indicate that the annual mean northwards ice transport from the Weddell Sea Gyre is of the order of 0.072 +/- 0.02 Sv. When we compare this interannual variability with the year-to-year statistics of mean drift from results shown in Figure 5 there appears only a weak correlation between Weddell Sea meridional transport and northward ice volume flux. Since sea ice does not reside in the Weddell Sea basin for much longer than 1 year, the total volumes of freshwater transport are likely determined more directly by short-term ice dynamics and deformation-related thickening than is the case for the export of the old, perennial Arctic ice pack. For instance, years with significant negative anomaly in ice extent appear to precede the largest anomalies in ice volume transport. Stagnant ice motion in 1990, although not contributing directly to a negative freshwater export anomaly that year, appears to facilitate the large quantity of thick ice exiting in the following year of 1991.

Linked to this variability is the strength of the south-westward ice transport into the eastern boundary of the Weddell Sea. This component of ice import in the east-wind drift amounts to a long-term mean of approximately 0.027 +/- 0.01 Sv. Clearly, the difference between the import and export terms imply a net production and export of ice of approximately 0.046 +/- 0.02 Sv. A 19 year time-series from 1979 to 1997 implies minima of 0.03 and 0,032 in 1985 and 1996, respectively and a maximum of 0.056 in 1991.

Salt production by freezing, during high mass export years must be balanced by melting of ice shelves and sea ice, precipitation, and the advection of fresher water in from the east in the Gyre circulation. Recent estimates show that the contribution of the Filchner-Ronne ice shelf front is only of the order of 90 km^3/yr or 0.03 Sv (Grosfeld and Gerdes, 1998), and that the sum of all contributions from ice shelf melting amounts to a total of approximately 0.01 Sv. If estimates of local <P-E> of 0.02 Sv (Bromwich *et al.*, 1997) are used for the entire Weddell Sea then the residual difference of approximately 0.02 Sv of freshwater must be balanced by freshwater advection. This implies that the entire Gyre dynamics adjust to the freshwater export on similar time scales, and that the greater net production of sea ice during strong export years, must be balanced by a net inflow of freshwater in the Antarctic coastal current.

These results demonstrate that the coupling of atmosphere and ocean takes place through the advective flux of freshwater in its ice phase. Clearly other regions such as the Weddell and Ross Seas participate in similar exchanges of momentum and heat and freshwater, and can have an equally significant impact in terms of their forcing of seasonal-interannual variability in the thermohaline circulation.

8. CONCLUSIONS

A strong oceanic response can be achieved via temporary redistribution of the surface freshwater flux at high latitudes through ice transport. In particular, pulses in ice export from the high latitudes also represent increased ice production and a more saline mixed layer, while the sub-polar Gyre becomes freshened and cooled by ice melt. Seasonally focused export of several hundreds of cubic kilometers of ice from the Arctic can have a considerable short term impact on the strength of the meridional overturning cell, with as much as 20% change in strength experienced during the Great Salinity Anomaly (GSA). Simulated meridional heat transport changes associated with such a event are of the order of 0.2 x 10^{15} Watts [Hakkinen, 1999]. If the same ice export had been distributed equally throughout the year, the same overturning response would likely not have been achieved, and thus the amplitude, duration and timing of the freshwater export are critical to the thermohaline response of the sub-polar gyre. Importantly though, the polar oceans also have a restoring capability through negative feedbacks in the system. Sea-ice growth rapidly replaces removed ice and brine production increases during this period. Consequently, the Arctic mixed layer becomes resalinated after exaggerated export years. The signal of these relatively saline, preconditioned waters eventually reaches the Labrador Sea to restart the convection process, thereby returning the system to more normal conditions.

Collective results from the Arctic and Antarctic illustrate that significant improvements are about to be realized in our estimates of these surface fluxes with existing and forthcoming satellite data sets. Future

widespread application of these satellite sea-ice products will help identify the accuracy and limitations of these new approaches. Furthermore, their use in concert with judiciously deployed ocean instrument technologies including; instrumented buoys, ULS, current meters, and hydrographic moorings, and fine-resolution GCMs will insure the most accurate quantification of surface fluxes. Together satellite remote sensing and 'in-situ' data sets will undoubtedly contribute to a new understanding of the impact of the polar oceans on climate and the global thermohaline circulation.

ACKNOWLEDGEMENT

This work has been undertaken at the Jet Propulsion Laboratory under contract to the National Aeronautics and Space Administration. Kim Partington of NASA Code Y kindly funded this research through research awards 665-21-02 (MRD); 621-21-02 (MRD); and 622-82-31 (MRD). CG acknowledges support from NSF grant OPP 9818645. The WCRP International Antarctic Buoy Programme, and its participants are acknowledged for use of their buoy data.

REFERENCES

Aagaard, K., and E.C. Carmack, The Role of Sea Ice and Other Fresh Water in the Arctic Circulation, *J. Geophys. Res.*, 94, C10, 14485-14498, 1989.

Agnew, T., H. Le, T. Hirose, Estimation of Large-Scale Sea-Ice Motion from SSM/I 85.5 GHz imagery, *Ann. Glaciology*, 25, 305-311, 1997.

Baranov, G.I., V.O. Ivchenko, M.I. Maslovskii, A.F. Treshnikov, and D.E. Kheisin, Wind Drift of Antarctic Sea Ice. In A.F. Treshnikov (Ed.) *Problems of the Arctic and Antarctic*, 47, 136-159, 1976.

Cavalieri, D.J., P. Gloersen, C.L. Parkinson, J.C. Comiso, ad H.J. Zwally, Observed Hemispheric Asymmetry in Global Sea Ice Changes, *Science*, 278, 1104-1106, 1997.

Dickson, R.R., J. Meincke, S.-A. Malmberg, and A.J. Lee, The "Great Salinity Anomaly", in the Northern Atlantic, 1968-1982, *Progr. Oceanography*, 20, 103-151, 1988.

Drinkwater, M.R., Satellite Microwave Radar Observations of Climate-Related Sea-Ice Anomalies, P*roc. Workshop on Polar Processes in Global Climate*, 13-15 Nov., 1996, 115-118, Am. Met. Soc., 1997.

Drinkwater, M.R., Satellite Microwave Radar Observations of Antarctic Sea Ice. In C. Tsatsoulis and R. Kwok (Eds.), *Analysis of SAR Data of the Polar Oceans*, 8, 147-187, Springer-Verlag, Berlin, 1998a.

Drinkwater, M.R., Active Microwave Remote Sensing Observations of Weddell Sea Ice. In M.O. Jeffries (Ed.) Antarctic Sea Ice: Physical Processes, Interactions and Variability, *Antarctic Research Series.*, 74, 187-212, American Geophysical Union, Washington, D.C., 1998b.

Drinkwater, M.R., and X. Liu, Active and Passive Microwave Determination of the Circulation and Characteristics of Weddell and Ross Sea Ice, *Proc. IGARSS '99*, Hamburg, Germany, 28 June - 2 July, 1999, IEEE Catalog # 99CH36293, Vol. 1, 314-316, 1999.

Drinkwater, M.R., X. Liu, J. Maslanik, and C. Fowler, Optimal Analysis Products Combining Buoy Trajectories and Satellite-Derived Ice-Drift Fields. International Programme for Antarctic Buoys, *IPAB Biennial Meeting Report, May 11-13, 1998, Naples, Italy*, WCRP Report No. 5/1999, p 1-11, World Climate Research Program, Geneva, Switzerland, 1999.

Emery, W.J., C.W. Fowler and J.A. Maslanik, Satellite-Derived Maps of Arctic and Antarctic Sea Ice Motion: 1988-1994, *Geophys. Res. Lett.*, 24, 8, 897-900, 1997.

Fily, M., and D.A. Rothrock, Sea Ice Tracking by Nested Correlations, *IEEE Trans. Geosci. and Remote Sens.*, GE-24, 6, 570-580, 1987.

Garreaud, R.D. and D.S. Battisti, Interannual (ENSO) and Interdecadal (ENSO-like) Variability in the Southern Hemisphere Tropospheric Circulation, *J. Climate*, 2113-2123, 1999.

Geiger, C.A., Y. Zhao, A.K. Liu, and S. Hakkinen, Large-Scale Comparison Between Buoys and SSM/I Drift and Deformation in the Eurasian Basin During Winter 1992-1993, *J. Geophys. Res.*, In Press.

Geiger, C.A., W.D. Hibler III, and S.F. Ackley, Modeled vs. Observed Drift and Deformation in the Western Weddell Sea During 1992, *J. Geophys. Res.*, 103, C10, 21893-21914, 1998.

Gloersen, P., W.J. Campbell, D.J. Cavalieri, J.C. Comiso, C. Parkinson, and H.J. Zwally, *Arctic and Antarctic Sea Ice, 1978-1987: Satellite Passive-Microwave Observations and Analysis*, SP-511, NASA Washington DC, 1992.

Hakkinen, S.M., A Simulation of Thermohaline Effects of a Great Salinity Anomaly, *J. Climate*, 12, 6, 1781-1795, 1999.

Harder, M., P. Lemke, and M. Hilmer, Simulation of Sea Ice Transport Through Fram Strait: Natural Variability and Sensitivity to Forcing, *J. Geophys. Res.*, 103, C3, 5595-5606, 1998.

Jacobs, S.S. and J.C. Comiso, Climate Variability in the Amundsen and Bellingshausen Seas. *J. Climate,* 10, 4, 697-709, 1997.

Johannessen, O.M., M.W. Miles, and E. Bjorgo, The Arctic's Shrinking Sea Ice, *Nature*, 376, 126-127, 1995.

Kottmeier, C., and L. Sellmann, Atmospheric and Oceanic Forcing of Weddell Sea Ice Motion, *J. Geophys. Res.*, 101, C9, 20809-20824, 1996.

Kwok, R. and D. A. Rothrock, Variability of Fram Strait Flux and North Atlantic Oscillation, *J. Geophys. Res.*, 104(C3), 5177-5189, 1999.

Kwok, R., J.C. Curlander, R. McConnell, and S.S. Pang, An Ice-Motion Tracking System at the Alaska SAR Facility, *IEEE J. Oceanic Eng.*, OE-15, 1, 44-54, 1990.

Kwok, R., A. Schweiger, D.A. Rothrock , S. Pang, and C. Kottmeier, Sea Ice Motion from Satellite Passive Microwave Imagery Assessed with ERS SAR and Buoy Motions. *J. Geophys. Res.*, 103, C4, 8191-8214, 1998.

Kwok, R., D. A. Rothrock, H. L. Stern and G. F. Cunningham, Determination of Ice Age using Lagrangian Observations of Ice Motion, *IEEE Trans. Geosci. Remote Sens.*, 33, 2, 392-400, 1995.

Kwok, R., G. Cunningham, N. LaBelle-Hamer, B. Holt, and D. A. Rothrock, Ice Thickness from High-Resolution Satellite Imagery, *EOS*, Transactions of the AGU, In Press.

Li, S., Z. Cheng, and W.F. Weeks, Extraction of Intermediate Scale Sea Ice Deformation Parameters from SAR Ice Motion Products. In C. Tsatsoulis and R. Kwok (Eds.), *Analysis of SAR Data of the Polar Oceans*, 8, 69-90, Springer-Verlag, Berlin, 1998a.

Liu, A., and D.J. Cavalieri, On Sea Ice Drift from the Wavelet Analysis of DMSP SSM/I data, *Int. J. Remote Sens.,* 19, 7, 1415-1423, 1998.

Liu, A., Y. Zhao, and S.Y. Wu, Arctic Sea Ice Drift from Wavelet Analysis of NSCAT and SSM/I data, *J. Geophys. Res.*, 104(C5), 11529-11538, 1999.

Long, D.G., and M.R. Drinkwater, Cryosphere Applications of NSCAT Data, *IEEE Trans. Geosci. and Remote Sens.*, Vol. 37, No. 3, 1671-1684, 1999.

Manabe, S., M.J. Spelman, R.J. Stouffer, Transient Responses of a Coupled Ocean-Atmosphere Model to Gradual Changes in Atmospheric CO2: Part II -Seasonal Response, *J. Climate*, 5, 105-126, 1992.

Maslanik, J.A., M. Serreze, and R.G. Barry, Recent Decreases in Arctic Summer Ice Cover and Linkages to Atmospheric Circulation Anomalies, Geophys. Res. Lett., 23, 13, 1677-1680, 1996.

Maslanik, J.A., C. Fowler, J. Key, T. Scambos, T. Hutchinson, and W. Emery, AVHRR-based Polar Pathfinder Products for Modeling Applications, *Ann. Glaciol.*, 25, 388-392, 1998.

Rudberg, A., T. Vinje, and T.B. Loyning, The Fate of Fram Strait Ice Fluxes, *ACSYS Arctic Forecast Newsletter*, 1, ISSN: 1028-2114, Polar Environmental Center, Tromso, Norway, 1999.

Stern, H.L., D.A. Rothrock, and R. Kwok, Open Water Production in Arctic Sea Ice: Satellite Measurements and Model Parameterization, J. Geophys. Res., 100(C10), 20601-20612, 1995.

Thorndike, A.S, and R. Colony, Large-scale Ice Motion in the Beaufort Sea During AIDJEX, April 1975 - April 1976. In *Sea Ice Processes and Models*, (Ed.) R.S. Pritchard, Univ. Washington Press, 249-260, 1980a.

Thorndike, A.S, and R. Colony, *Arctic Ocean Buoy Program, 19 January 1980 - 31 December, 1979*, Report, Polar Science Center, University of Washington, Seattle, 1980b.

Thorndike, A.S, and R. Colony, Sea Ice Motion in Response to Geostrophic Winds, *J. Geophys. Res.*, 87, C8, 5845-5852, 1982.

Vinje, T., and O Finnekasa, The Ice Transport Through the Fram Strait, Rep. 186, *Nor. Polarinst*., Oslo, Norway, 39pp. 1986.

Vinje, T., N. Norlund, and A. Kvambekk, Monitoring Ice Thickness in Fram Strait, *J. Geophys. Res.*, In Press.